JOURNAL OF MATERIALS SCIENCE 28 (1993) 6074–6080

Correlation of microhardness and morphology in injection-moulded poly(ethylene terephtalate)

F.J. BALTÁ CALLEJA, J. BARANOWSKA*, D.R. RUEDA
Instituto de Estructura de la Materia, CSIC, Serrano 119, 28006 Madrid, Spain
R.K. BAYER
Institut für Werkstofftechnik, Universität GH Kassel, Wilhelmshöherallee 73, 3500 Kassel, Germany

Microindentation hardness has been applied to a series of injection-moulded poly(ethylene terephtalate) samples prepared using a range of mould temperatures, T_c. The morphology of the samples was characterized by X-ray diffraction and differential scanning calorimetry. Depending on T_c, it is shown that microhardness is lower at the surface than in the core of the mouldings. Results are discussed in terms of the volume fraction of spherulites filling the mouldings which is shown to be dependent upon T_c. The influence of an annealing treatment on the properties of the mouldings is examined. The microhardness values are correlated with the thickness and with the surface free energy of the lamellar crystals. The results obtained indicate that increasing annealing temperatures first leads to an increase and then to a sudden decrease of hardness. The latter can be associated with the changes occurring in the number of defects on the crystal's surface.

1. Introduction

In recent years investigations of the microhardness properties have emerged as a physical method which can provide a quantitative information on changes in the morphology of polymeric materials [1–3]. A large number of studies make reference to highly crystalline polymer materials [3]. A few investigations on microhardness of low-crystallinity materials and glassy polymers are also available [4–7]. In a recent study, the investigation of the microhardness of poly(ethylene terephtalate) (PET) has been reported in relation to the microstructure [8]. By varying the temperature and time of crystallization from the glassy state, different states of crystalline perfection can be frozen-in by quenching the sample to room temperature. Two main types of morphologies have been examined: (1) structures where spherulitic growth is incomplete resulting from a primary crystallization from the glassy state, as shown in Fig. 1a; (2) structures in which spherulitic crystallization is completed (Fig. 1b). We have shown that for the former materials, H, the hardness, increases, depending on annealing time, with the volume fraction of spherulites, from $H \simeq 120$ MPa for the glassy material up to $H \simeq 200$ MPa for the material fully occupied with spherulites. For these materials [8]

$$H = H_{sph}\phi + H_a(1 - \phi) \quad (1)$$

where H_{sph} and H_a are the hardness of spherulitic and interspherulitic ("amorphous") material, respectively, and ϕ is the volume fraction of spherulites.

For materials in which spherulitic growth is completed, H remains nearly constant with increasing temperature of annealing, T_a. For this second class of materials the microhardness of spherulitic PET can be correlated to the microstructure through the following expression [8]

$$H_{sph} = H_c\alpha_L + H_a(1 - \alpha_L) \quad (2)$$

where

$$H_c = H_o/[1 + (b/l_c)] \quad (3)$$

is the hardness of the crystals having a thickness l_c, H_a the hardness of the amorphous regions and $\alpha_L = l_c/L$ is the linear crystallinity. H_o in Equation 3 represents the hardness for infinitely thick crystals and b is a parameter which measures the hardness depression from H_o; b has been shown to be equal to $2\sigma/\delta h$ (σ is the surface free energy of crystal lamellae, and δh the energy of crystal destruction) [8].

The purpose of the present work was to study the mechanical properties of injection-moulded PET. It is known that process variables induce substantial changes in the microstructure of the moulded material [9]. Variations often occur in the plane surfaces and across the thickness of the moulded samples. As a result, the mechanical properties can be governed by

* *Present address*: Faculty of Engineering, Technical University of Szczecin, Poland.

0022–2461

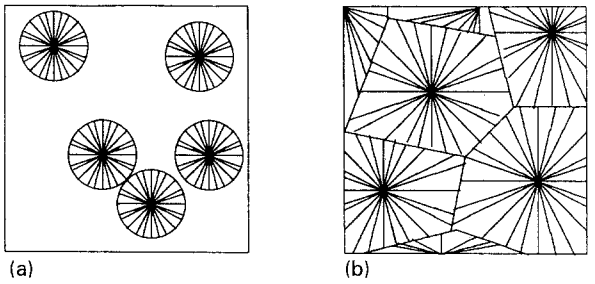

Figure 1 Schematic representation of the morphology in spherulitic crystallized PET for (a) an incompleted spherulitic growth, (b) a completed spherulitic crystallization.

various variables such as melt and mould temperature, injection pressure, ageing, etc. [10]. In a recent study [11–13], it was shown that the processing conditions of injection-moulded polyethylene using an extensional flow component strongly influence physical properties such as yield strength, density, shrinkage behaviour, microhardness, etc. The object of this investigation is to extend our previous studies to the correlation between process variables, microstructure and mechanical properties of injection-moulded PET by means of a combined microhardness, differential scanning calorimetry (DSC) and X-ray diffraction (XRD) study. In this paper the results of microhardness variations occurring across the moulding thickness will be reported and the influence of a thermal treatment of the original material in the form of pellets, on the properties of the mouldings will be analysed. The effect of an annealing treatment on the microhardness of the mouldings will also be examined.

2. Experimental procedure

2.1. Materials and processing conditions

Commercial poly(ethylene terephtalate) (PET), with a weight average molecular weight of $M_w = 29800$ (Hoechst) in the form of pellets was used to prepare the injection-moulded materials. The molecular weight of the pellets was measured by viscometry in the laboratory of Professor. H.G. Zachmann, Hamburg. In a first series of injection-moulding experiments, PET pellets were used as-supplied (Samples A). In a second series of experiments, samples were prepared after drying the pellets at 150 °C under rotary pump vacuum for 3 h (Samples B). The M_w value of the dried pellets was 31300. The injection-moulded materials were obtained using a Klöckner Ferromatic FM 85 injection moulder. The melt temperature was $T_m = 285$ °C and the injection pressure 400 bar. Different temperatures of the mould, T_c from 25–150 °C, were used. Two different geometries for the mould were employed: (a) a conventional dumb-bell shape mould having a $4 \times 10\ mm^2$ (xy) cross-section [10]; (b) a two-arm elongational flow mould with a $4 \times 4\ mm^2$ cross-section [11, 12]. The bars prepared at low temperatures show a transparent skin whose thickness is the higher, the lower is the mould temperature. To investigate the gradient of properties and the varying morphology present in the injected bars, half of each bar (at $x = 2$ mm) was removed to obtain a smooth flat yz surface, in which to carry out microhardness and XRD measurements (see Fig. 2). Annealing treatments at different temperatures, T_a, of these half bars were carried out in an oven under rotary pump vacuum for 1 h.

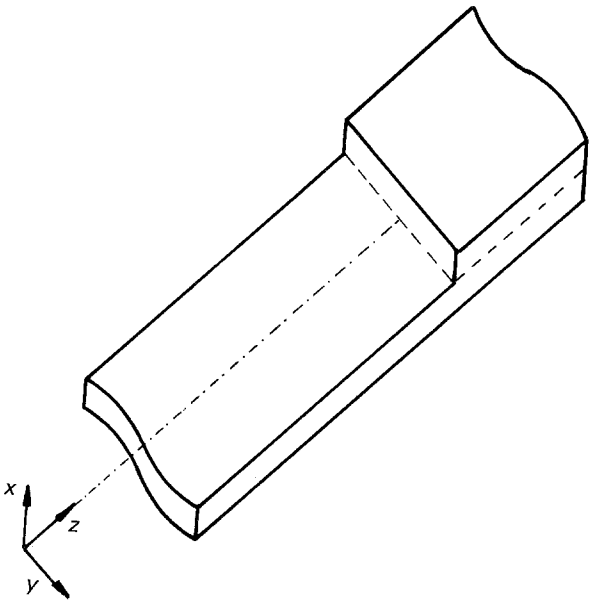

Figure 2 Geometry of the injection-moulded PET bar. z, injection direction; x, normal to the bar surface. Indentations were made on the yz plane.

2.2. Techniques

2.2.1. X-ray diffraction

Preliminary transmission wide-angle X-ray diffraction (WAXD) patterns, were obtained to verify a possible orientation throughout the thickness of the samples. Because no orientation was observed in any of the samples investigated, a diffractometer was used to obtain XRD scans from the inner surface (yz plane at $x = 2$ mm) of the centre part of the bars. CuK_α radiation, filtered with nickel, was used. A goniometer speed of $1\ °(2\theta)\,min^{-1}$ and a recorder speed of 1 cm min^{-1}, respectively, were used. Crystallinity values, x_c, were determined as the ratio of the crystalline area to the total area observed between 5 ° and 37 °(2θ) after subtraction of the background. A curve analyser was used to resolve the crystalline peaks observed in the diffractograms. Crystallite size dimensions, D_{hkl}, along the [010] and [100] crystallographic directions, were calculated from the integral-breadth value, δβ, using the approximation $\delta\beta \approx 1/D_{hkl}$, after correction for instrumental line broadening [14]. Small-angle X-ray scattering (SAXS) patterns were obtained with a point collimation Kiessig camera using a sample–film distance of 400 mm. A copper-rotating anode X-ray generator with a fine focus working at 40 kV and 70 mA was used. Well-defined isotropic scattering maxima were observed. The long spacings were calculated from densitometric profiles after continuous scattering subtraction and correction by the Lorentz factor.

2.2.2. Hardness and calorimetry measurements

A Leitz microhardness tester with a square-based

TABLE I Crystallinity, x_c, long period, L, microhardness, H, and b of injection-moulded PET as function of T_c

Sample	T_c (°C)	x_c (%)	L(nm)	H(MPa)	b(nm)
A1	25	25	9.6	192	5.3
A2	90	29	8.8	195	4.9
A3	130	29	10.3	200	5.7
A4	150	29	9.9	202	5.5
B1	25	14	10.7	165	6.0
B2	90	23	9.9	176	5.5
B3	130	28	10.1	190	5.6

diamond indentor was used for the surface-microhardness measurements. Microhardness, H, was calculated from the indentation diagonal value, d(μm), according to the expression $H = kP/d^2$ (MPa), where $k = 18180$ is a geometrical constant. A load, P, of 0.2 N and a loading cycle of 6 s were used. Each H value corresponds to the mean of five measurements carried out on a small area, along the z-axis on the surface investigated. A differential scanning calorimeter, Perkin–Elmer DSC-4 was used. The DSC curves were recorded using a heating rate of 10 K min^{-1}. The weight of the sample was about 5 mg. The melting temperature measured from the peaks of traces was calibrated against indium.

3. Results

3.1. Injection-moulded samples

Preliminary visual observations of the injection-moulded bars reveal that for a given mould temperature, T_c, Samples B (using dried pellets) show a transparent skin which is thicker than that in Samples A (using pellets as supplied; Table I). Such a transparent skin is not observed in Samples A for T_c values higher than 90 °C. Transmission XRD patterns indicate the absence of orientation throughout the thickness of the injected bars, even for those with the smallest cross-section. Consequently, the following results will be concerned only with samples having the largest cross-section ($y = 10$ mm) (Samples A and B).

Fig. 3 shows the H values measured on the outer surface of the bars for the two series of samples (A and B). Most remarkable is the sudden increase in H from ≈ 120 MPa up to 200 MPa observed for samples prepared with T_c values above 120 °C.

Fig. 4 shows the DSC traces for Sample B1 obtained from slices of the bar taken at different values of y (with $x \approx 2$ mm). An endothermic peak at about 260 °C, which corresponds to the melting of the crystalline polymer, is present in all the DSC curves. In addition, an exothermic peak at about 120 °C is observed, particularly for material portions closer to the external surface of the injected bar. This exothermic peak corresponds to the crystallization of the amorphous PET regions.

Table I shows the values of crystallinity obtained by XRD, x_c, the X-ray long period, L, and the microhardness, H, measured at the inner surface of the bars (mean value observed for $y = 4$–6 mm) as a function of T_c. In Fig. 5 it is seen that the values of H for

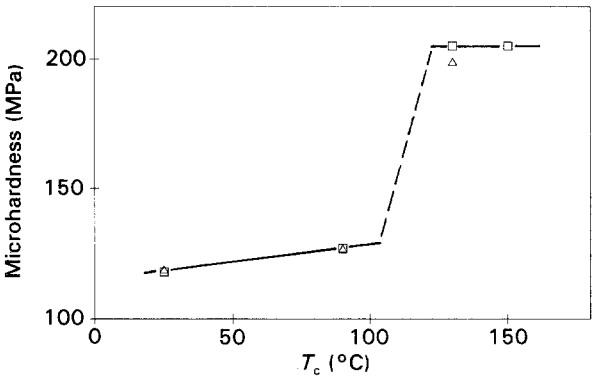

Figure 3 Microhardness measured on the outer surface of the PET bar injected at different mould temperatures, T_c.

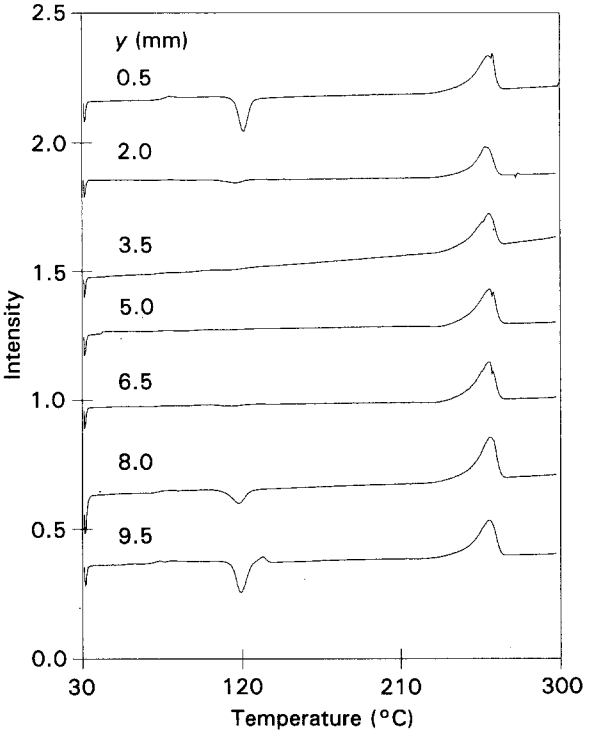

Figure 4 DSC traces for Sample B1 obtained from cuts of the bar at different y-values.

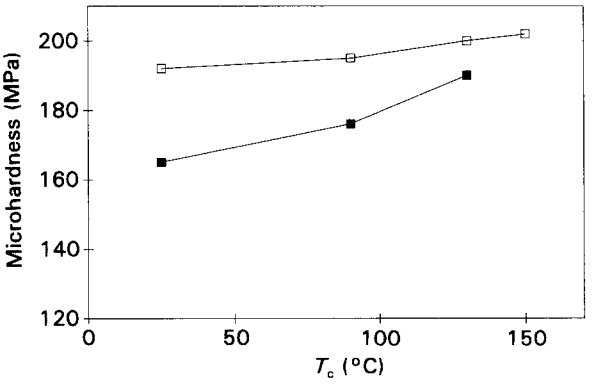

Figure 5 Microhardness measured at the inner yz surface (at $x = 2$ mm) of PET bars processed at different T_c. (□) Samples A, (■) Samples B.

Samples A are larger than for the Samples B. This is connected to the fact that the x_c values for the former are larger than for the latter samples (Table I). Fig. 5 additionally illustrates the clear influence of the mould

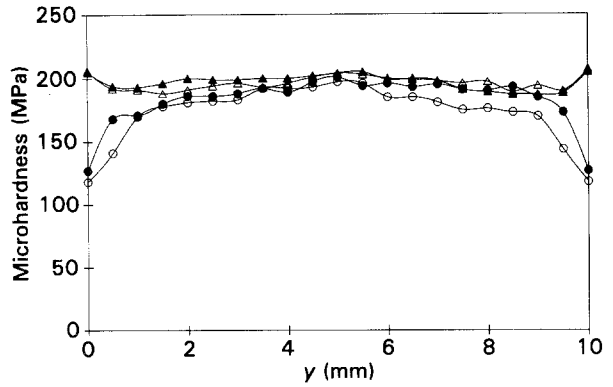

Figure 6 Microhardness profiles along the *y*-direction obtained from measurements at the inner *yz* surface of Samples A. (○) A1, (●) A2, (△) A3, (▲) A4.

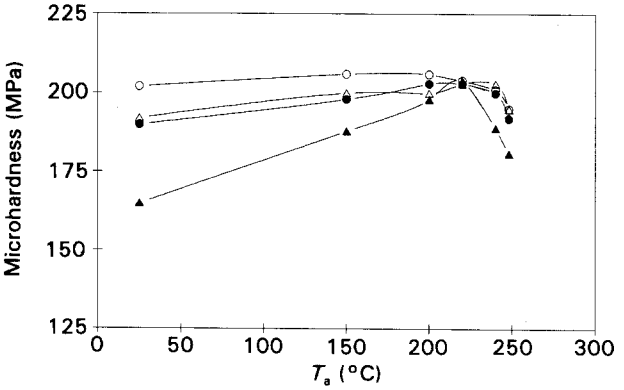

Figure 8 Variation of H with T_a for the annealed injection-moulded materials. (△) A1, (○) A4, (▲) B1, (●) B3.

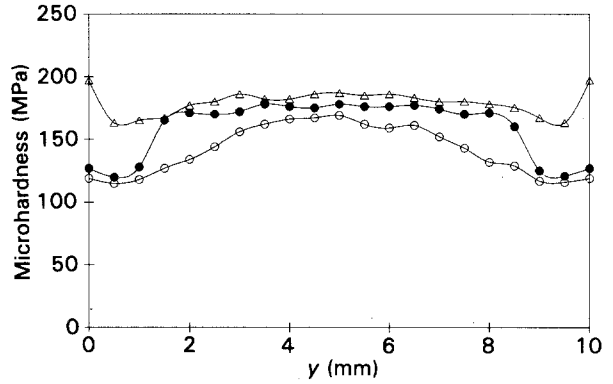

Figure 7 Microhardness profiles along the *y*-direction obtained from measurements at the inner *yz* surface of Samples B. (○) B1, (●) B2, (△) B3.

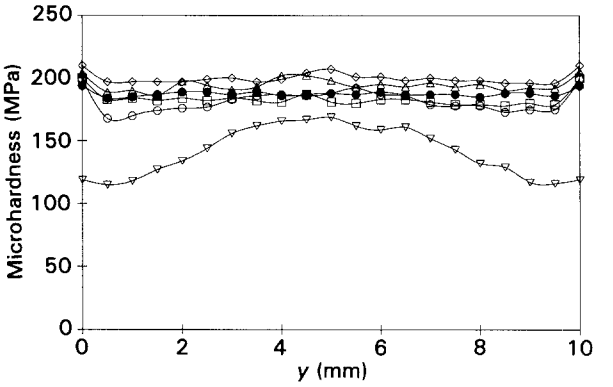

Figure 9 Microhardness profiles along the *y*-direction for Sample B1 before and after annealing at different temperatures T_a. (▽) Unannealed, (○) 150 °C, (□) 200 °C, (△) 220 °C, (◇) 240 °C, (●) 248 °C.

temperature on the values of H measured at the inner *yz* surface. The fact that the values of H obtained in all samples are lower than 200 MPa suggests that in these materials the spherulitic structure is not completed ($0.4 < \phi < 0.8$). Figs 6 and 7 show the H values observed on the inner *yz* surface across the thickness of the moulding (*y*-direction) for the two series of Samples A and B, respectively. The values of the mechanical parameter, b, calculated by means of Equation 3, assuming for $H_o \approx 420$ MPa [15], $H_c \approx 230$ MPa [8] and $l_c = 0.7L$ [16] are also given in Table I. It is seen that for the injection-moulded samples, b is independent of T_c.

3.2. Influence of annealing

Table II shows the X-ray crystallinity, x_c, the crystallite size values, D_{hkl}, along the [010] and [100] crystallographic directions, the long period, L, and the values of H and b as a function of annealing temperature, T_a. An increase of crystallinity with T_a is typically observed up to $T_a = 240$ °C, followed by a small decrease for the highest T_a investigated. With reference to microhardness (see Fig. 8), while Sample A4 is unaffected by the annealing treatment up to ≈ 220 °C, because it initially shows a completed spherulitic structure, the rest of the samples exhibit a continuous hardening with increasing T_a. Most remarkable is the clear tendency for H to decrease, observed for the highest T_a investigated.

Fig. 9 illustrates the microhardness profiles measured, across the moulding thickness, along *y*, on the inner *yz* surface for one of the B samples ($T_c = 25$ °C) before and after annealing at different temperatures. After annealing at 150 °C, a notable hardening is observed throughout the thickness of the sample, being maximum on the outer surface. It is worth noting that the ≈ 1.5 mm thick amorphous skin detected for the untreated sample hardens after the treatment at $T_c = 150$ °C. For higher annealing temperatures, H reaches a similar limiting value of about 200 MPa throughout the thickness of the samples.

Fig. 10 shows the plot of the long period, L, as a function of T_a. For samples injected at low T_c one observes first a decrease of L with T_a up to $T_a \simeq 200$ °C and then a conspicuous increase in L. In the case of samples processed at high mould temperatures, L remains nearly constant up to $T_a = 200$ °C and then it increases rapidly with T_a.

Fig. 11 comparatively depicts L together with the crystal size values, $D_{0\,1\,0}$ and $D_{1\,0\,0}$, for one of the samples (A4) as a function of T_a. The $D_{0\,1\,0}$ and $D_{1\,0\,0}$ values here remain constant up to $T_a = 200$ °C and, finally rise with T_a following a parallel increase with L. A similar behaviour of L, $D_{0\,1\,0}$, and $D_{1\,0\,0}$ was found for the rest of the annealed samples.

Fig. 12 shows the DSC traces for one of the samples (A4) before and after annealing treatment at various temperatures. It is noteworthy that both the position

TABLE II Crystallinity, x_c, crystallite size, D, long period, L, microhardness, H, and b for various mouldings before and after annealing at different T_a for 1 h

Sample	T_a (°C)	x_c (%)	D_{010} (nm)	D_{100} (nm)	L (nm)	H (MPa)	b (nm)
A1	25	25	7.1	6.1	9.6	192	5.3
	150	28	7.1	6.1	7.7	200	4.4
	200	32	7.8	6.3	8.5	200	4.7
	220	34	8.7	6.3	9.5	203	5.3
	240	35	12.1	8.9	10.6	203	5.9
	248	36	13.0	9.6	13.4	195	7.4
A4	25	29	8.3	6.1	9.9	202	5.5
	150	31	8.3	6.4	10.0	206	5.6
	200	31	8.3	6.6	9.9	206	5.5
	220	31	8.7	7.2	9.7	204	5.5
	240	35	12.7	9.4	12.2	201	6.8
	248	34	14.0	10.4	14.5	195	8.1
B1	25	14	7.1	5.5	10.7	165	6.0
	150	29	7.1	5.5	8.5	188	4.7
	200	32	7.5	5.5	8.8	198	4.9
	220	34	9.2	6.1	9.6	204	5.3
	240	36	12.1	8.4	11.2	189	6.2
	248	32	13.6	10.4	14.0	181	7.8
B3	25	28	7.5	5.7	10.1	190	5.6
	150	31	7.5	5.9	9.5	198	5.3
	200	32	7.9	5.9	10.1	203	5.6
	220	34	9.2	6.4	11.4	203	6.3
	240	36	11.1	8.7	12.7	200	7.1
	248	35	13.3	10.0	–	192	–

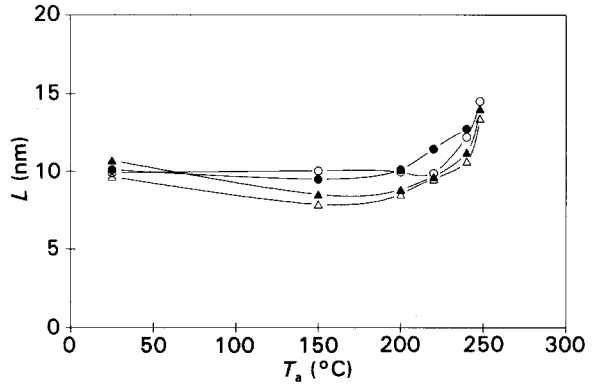

Figure 10 Variation of the long period of injected PET bars as a function of annealing temperature. (△) A1, (○) A4, (▲) B1, (●) B3.

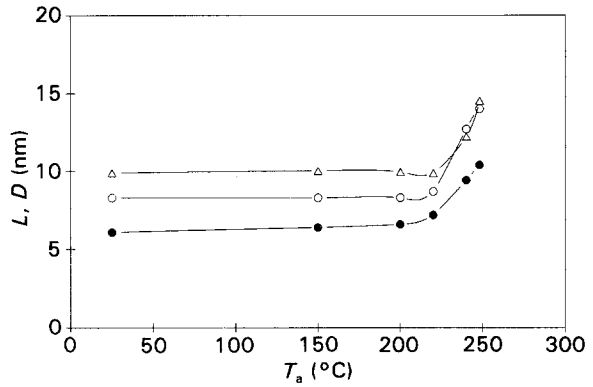

Figure 11 Variation of (△) the long period and crystallite size values (○) D_{010} and (●) D_{100} of Sample A4 with T_a.

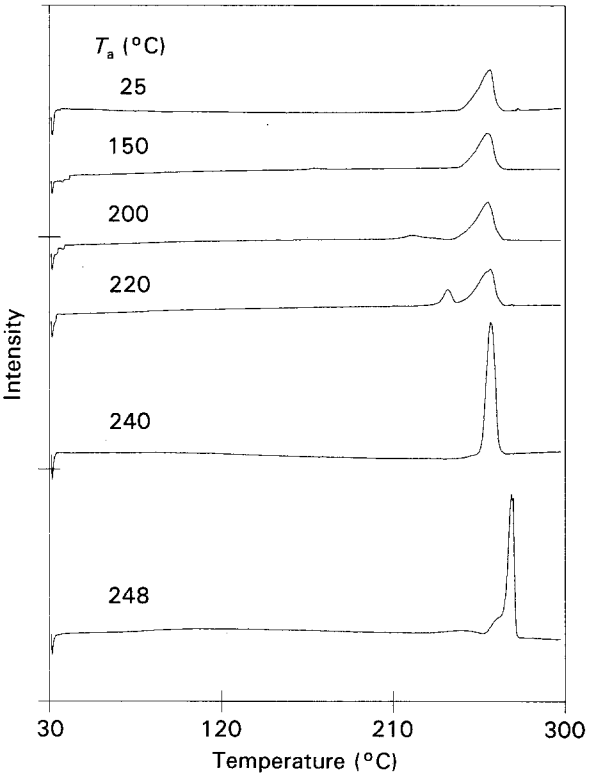

Figure 12 DSC traces from the core of injected bars of Sample A4 before and after annealing at different temperatures.

and the shape of the dominant endothermic peak corresponding to the melting of the polymer do not change appreciably for $T_a \leq 220\,°C$. A new endothermic peak due to the annealing treatment appears at about 15–20 K above the T_a value used. The intensity of this new peak (annealing peak) increases with T_a. For $T_a = 240\,°C$ the annealing peak seems to coincide with the dominant endothermic peak. Finally, for $T_A = 248\,°C$ both maxima shift together to about 20 K above T_a.

4. Discussion

As pointed out above, despite using injection moulding with an extensional flow mould, neither molecular orientation nor lamellar orientation could be achieved. This is probably due to the low viscosity of the material used, even for the dried samples. Thus we shall limit our discussion to the series of samples processed using the largest cross-section mould.

In the first place it is noteworthy that the DSC scans of thin cuts across the thickness of Sample B1 show an exothermic peak of crystallization which preferentially characterizes the amorphous material located on the outer surface (Fig. 4). As expected, a transition in H from the amorphous state ($H_a = 120$ MPa) into the fully spherulitic semicrystalline material ($H_{sph} \approx 200$ MPa) is obtained on the outer surface of the bars around a crystallization temperature $T_c = 120\,^{\circ}C$ (Fig. 3). A similar transition in H has been reported for compression moulded PET [8].

On the other hand, DSC curves from the inner cuts show very small exothermic recrystallization peaks suggesting that the interior of the mouldings is crystallized to a great extent. Indeed, the mechanical measurements carried out in the centre of the mouldings (Fig. 5) show H values between 120 and 200 MPa, corresponding to materials partially filled with spherulites [8]. In addition, all the cuts show an endothermic peak at about 260 °C due to the fusion of the crystallized material.

Furthermore, the results in Fig. 5 suggest that the mouldings of Samples A show a more completed spherulitic growth (higher H values) than mouldings of Samples B. The reason for the lower values of H in Samples B might be sought in an increase of molecular weight after drying the initial pellets, thus hindering the crystallization process. In addition, the gradual improvement of hardness with increasing T_c, obtained for both types of samples, is presumably due to an increasing volume fraction of spherulitic material. For the samples processed at $T_c = 25\,^{\circ}C$ due to the slow rate of crystallization of PET, the crystallization in the centre of the bar is not as complete as in the case of $T_c = 120\,^{\circ}C$ where cooling proceeds more slowly. Therefore, in the case of $T_c = 25\,^{\circ}C$ the samples are only partially filled with spherulites showing values of less than 200 MPa.

Fig. 6 shows the H profile across the y-dimension for Samples A supporting the presence of an outer amorphous layer in the samples with T_c below 120 °C. However, on increasing T_c above 120 °C, the amorphous layer crystallizes and hardens. It should be noted that for the samples prepared at $T_c \geq 120\,^{\circ}C$, H shows a distinct maximum at both surfaces, suggesting the enhancing nucleation effect of the metallic walls of the mould on the crystallizing material. A similar H profile, for Samples B, is shown in Fig. 7, but, with H values smaller than 200 MPa, indicating that crystallization is not as complete as in the case of Samples A (see also Figs 4, 5 and Table I). In this latter case, we also observe an increase in H near the surface due to the above mentioned wall effect.

It is worth noting that the values of b derived for Samples A, are indistinguishable from those for Samples B (Table I). The high b values obtained in contrast with previous results on melt-crystallized samples [8] suggest the occurrence of a higher surface free energy which is probably connected with a higher concentration of entanglements and defects at the crystal surface.

We have seen that the use of low mould temperatures specially in the case of Samples B, leads to mouldings with low H values where primary crystallization is not completed (Table I). One way to improve the properties of the injection-moulded material is by means of a subsequent annealing treatment at temperatures, T_a, well above 120 °C. The influence of annealing upon the H profile of Sample B prepared at $T_c = 25\,^{\circ}C$ is remarkable at all T_a values (Fig. 9). At $T_a = 150\,^{\circ}C$, H has already reached values of 180 MPa which correspond to a volume fraction of spherulites $\phi \simeq 0.8$ [8]. For the highest annealing temperatures used, an homogeneous hardening across the sample ($H \simeq 200$ MPa) corresponding to a completed primary crystallization is obtained. The slightly higher H values measured on the surface, corresponding to the mould wall effect, are also reflected in slightly higher H values at the surface of the corresponding annealed materials.

One specific feature of the PET microstructure is that L increases linearly with T_a [17] and that the linear crystallinity $\alpha_L = l_c/L$ shows a nearly constant value equal to 0.7 in the annealing range of 120–250 °C [16]. Unexpectedly, we obtain for all the samples a variation of L as a function of T_a (Fig. 10) which clearly deviates from such a linear behaviour observed for PET crystallized from the glassy state [16]. In order to explain this result it is convenient to discuss the DSC data for Sample A4 ($T_c = 150\,^{\circ}C$) annealed at the different temperatures (Fig. 12). The initial injection-moulded sample shows just one single endothermic peak at 260 °C. One has to assume that the poorly crystallized sample recrystallizes during heating and that the melting peak corresponds to the melting of the recrystallized material [18]. The annealed mouldings present an additional smaller endothermic peak at roughly $T = T_a + 20$. This second peak suggests the presence of a fraction of additional lamellae which are crystallized at T_a. The presence of a fraction of these lamellae in the temperature range 150–220 °C may contribute to a reduction of the stacking periodicity of the initial crystal lamellae yielding the observed decrease of L in Fig. 10. However, for T_a values larger than 220 °C, annealing results in a thickening of the original lamellae giving rise to both an increase of L and an increase of the melting peak.

It must be pointed out that a decrease of L is also found during isothermal crystallization [19, 20] and may be explained in the same way by the formation of additional lamellae. The decrease of L is specially noticeable in the samples processed at $T_c = 25\,^{\circ}C$ (Fig. 10), having initially a larger volume of amorphous material (see Figs 5 and 7) which is susceptible to crystallization . The parallel increase of L (proportional to the thickness of the crystals) and D_{010} and D_{110} suggest that the crystal thickening also entails a

volume increase of the crystals with T_a (Fig. 11). Finally, a hardness increase with annealing temperature is observed until a value of about $T_a = 220\,^{\circ}C$ is reached (Fig. 8). However, for higher T_a values, H suffers an unexpected decrease. The hardness behaviour can be understood if we examine the variation of b with T_a (Table II). Because for annealed PET, $l_c \simeq L$ [8], from Equation 3 it follows that b must be proportional to L in the T_a range investigated. This explains the initial decrease of b with T_a (this could be associated with the presence of thin lamellae within the stacks), and the final increase of this parameter for $T_a > 220\,^{\circ}C$. These results suggest that the density of defects on the crystal surface (proportional to b) first decreases due to the presence of the thin lamellae (L decrease in Fig. 9) and that, at higher temperatures, T_a, the number of defects increases with increasing crystal thickness causing, as a result, the hardness of the material to decrease. Particularly for $T_a = 248\,^{\circ}C$, it is seen that some molten material recrystallizes at lower temperatures (contributing to less-perfect crystals) (Fig. 12) in support of the observed increase of the constant b (hardness decrease) (see Table II).

Acknowledgements

The authors thank CICYT (grant MAT 90-0795), Spain, for generous support of this investigation. J. B. is indebted to the Tempus Program (JEP 0644) for supporting her investigation by a grant. We are grateful to Professor H. G. Zachmann, University of Hamburg, for very valuable discussion concerning the interpretation of results and for the molecular weight determination of the investigated PET materials as mentioned in the text.

References

1. F. J. BALTÁ CALLEJA. *Adv. Polym. Sci.* **66** (1985) 117.
2. F. J. BALTÁ CALLEJA and H. G. KILIAN, *Colloid Polymer. Sci.* **263** (1985) 697.
3. F. J. BALTÁ CALLEJA, J. MARTÍNEZ SALAZAR, and D. R. RUEDA, in "Encyclopedia of Polymer Science and Engineering, Vol. 6 (Wiley, New York, 1986), p. 614.
4. F. ANIA, J. MARTÍNEZ SALAZAR and F. J. BALTÁ CALLEJA, *J. Mater. Sci.* **24** (1989) 2934.
5. Y. DESLANDES, E. ALVA ROSA, F. BRISS and T. MENEGHINI, *ibid.* **26** (1991) 2769.
6. F. J. BALTÁ CALLEJA, C. SANTA CRUZ, D. CHEN and H. G. ZACHMANN, *Polymer* **32** (1991) 2252.
7. R. H. ION, H. M. POLLOCK and C. ROGUES-CAMES, *J. Mater. Sci.* **25** (1990) 1444.
8. C. SANTA CRUZ, F. J. BALTÁ CALLEJA, H. G. ZACHMAN, N. STRIBECK and T. ASANO, *J. Polym. Sci. Polym. Phys.* **B29** (1991) 819.
9. F. JOHANNABER, "Injection-Moulding Machines", 2nd Edn (Hanser, New York, 1985) p. 39.
10. D. R. RUEDA, F. J. BALTÁ CALLEJA and R. K. BAYER, *J. Mater. Sci.* **16** (1981) 3371.
11. R. K. BAYER, H. G. ZACHMANN, F. J. BALTÁ CALLEJA and H. UMBACH, *Polym. Eng. Sci.* **29**(3) (1989) 186.
12. E. LÓPEZ CABARCOS, H. G. ZACHMANN, R. K. BAYER, F. J. BALTÁ CALLEJA and W. MEINS, *ibid.* **29**(3) (1989) 1983.
13. D. R. RUEDA, R. K. BAYER, F. J. BALTÁ CALLEJA and H. G. ZACHMANN, *J. Macromol. Sci. Phys.* **B28**(2) (1989) 265.
14. F. J. BALTÁ CALLEJA and C. G. VONK, "X-Ray Scattering of Synthetic Polymers" (Elsevier, Amsterdam, 1989).
15. O. ÖHM, R. K. BAYER and F. J. BALTÁ CALLEJA, unpublished work (1992).
16. C. SANTA CRUZ, N. STRIBECK, H. G. ZACHMANN and F. J. BALTÁ CALLEJA *Macromolecules* **24** (1991) 5990.
17. F. J. BALTÁ CALLEJA, C. SANTA CRUZ, R. K. BAYER and H. G. KILIAN, *Colloid Polym. Sci.* **268** (1990) 440.
18. H. G. ZACHMANN and R. GEHRKE, in "Morphology of Polymers", edited by B. Sedlacek (Walter de Gruyter, Berlin, New York, 1986) p. 119.
19. H. G. ZACHMANN and G. F. SCHMIDT, *Makromol. Chem.* **52** (1962) 23.
20. G. ELSNER, M. H. J. KOCH, J. BORDAS and H. G. ZACHMANN, *ibid.* **182** (1981) 1263.

Received 23 June 1992
and accepted 19 March 1993